

# EVALUATION OF SPECKLE REDUCTION WITH DENOISING FILTERING IN OPTICAL COHERENCE TOMOGRAPHY FOR DERMATOLOGY

Juan J. Gómez-Valverde<sup>1,2</sup>, Juan E. Ortuño<sup>2,1</sup>, Pedro Guerra<sup>1,2</sup>, Boris Hermann<sup>3</sup>, Behrooz Zabihian<sup>3</sup>, José L. Rubio-Guivernau<sup>4</sup>, Andrés Santos<sup>1,2</sup>, Wolfgang Drexler<sup>3</sup>, María J. Ledesma-Carbayo<sup>1,2</sup>

<sup>1</sup> Department of Electronic Engineering, ETSI Telecomunicación, Universidad Politécnica de Madrid, Spain

<sup>2</sup> Biomedical Research Center in Bioengineering, Biomaterials and Nanomedicine (CIBER-BBN), Spain

<sup>3</sup> Center for Medical Physics and Biomedical Engineering, Medical University of Vienna, Austria

<sup>4</sup> MedLumics S.L Tres Cantos (Madrid), Spain

## ABSTRACT

Optical Coherence Tomography (OCT) has shown a great potential as a complementary imaging tool in the diagnosis of skin diseases. Speckle noise is the most prominent artifact present in OCT images and could limit the interpretation and detection capabilities. In this work we evaluate various denoising filters with high edge-preserving potential for the reduction of speckle noise in 256 dermatological OCT B-scans. Our results show that the Enhanced Sigma Filter and the Block Matching 3-D (BM3D) as 2D denoising filters and the Wavelet Multiframe algorithm considering adjacent B-scans achieved the best results in terms of the enhancement quality metrics used. Our results suggest that a combination of 2D filtering followed by a wavelet based compounding algorithm may significantly reduce speckle, increasing signal-to-noise and contrast-to-noise ratios, without the need of extra acquisitions of the same frame.

**Index Terms**— Optical Coherence Tomography, speckle, denoising, dermatology

## 1. INTRODUCTION

Optical coherence tomography (OCT) is a non-invasive technique that presents an *in vivo* view of the superficial layers of tissue in real-time [1]. In scattering tissues OCT offers a penetration depth of 1–2 mm with typical axial and transverse resolutions between 1–10  $\mu\text{m}$  and approximately 20  $\mu\text{m}$ , respectively, depending on the wavelength region [2]. As a diagnostic tool, it is broadly used in ophthalmology since its introduction and its potential usefulness in other specialties like dermatology in the diagnosis of skin diseases [3] has been proved. In particular OCT has shown promising results as a non-invasive alternative to excisional biopsy helping in the detection of tumors, such as malignant melanoma and basal cell carcinoma, complementing other imaging tools such as dermoscopy or confocal laser scan microscopy [2, 4].

Speckle noise is the most prominent artifact present in the OCT images. It limits the interpretation and diagnosis and reduces both contrast and signal to noise ratio (SNR) [5]. In images of highly scattering biological tissues, speckle has a dual role as a source of noise and a carrier of

information on tissue microstructure. The signal-carrying speckle is generated by single back scattering of the incident light, while the signal-degrading speckle is generated due to interference of photons multiply scattered in reverse and forward direction [6]. The resulting speckle pattern is visible in the image as a grainy appearance which blurs structural detail information. Therefore special care should be taken, because removing the speckle could imply deleting useful information.

Much work has been performed for reducing speckle noise. We can make a first classification of speckle reduction techniques in software and hardware solutions [7]. The hardware based techniques require the modification of the optical setup or the scanning protocols. The goal is to obtain several tomograms that are averaged to obtain final images with a reduction in speckle contrast. The main challenge of these methods is to acquire images in a way that the speckle pattern changes, but produces a minimum alteration of the image structure. Other solutions try to acquire several B-scans in consecutive time intervals from the same location of the sample, but with a slightly changed ensemble of the illuminated scattering particles [7]. Another popular approach to differentiating speckle pattern is angular compounding, that consists in averaging tomographic images acquired from different observation angles [8]. Finally in the last few years several new methods have been proposed to improve the lateral resolution beyond the diffraction limit using structured interferences in a similar way as in confocal microscopy [9].

Software based speckle reduction techniques can be applied without modifying the acquisition configuration. The drawback is that they could need high computation requirements and could affect the resolution of the image or incorporate artifacts that may alter the interpretation of the features of interest. We can include in this group multiple methods like local averaging over all A-scans of each tomogram [10], averaging multiple B-scans [11], digital filtering the B-scans using digital filters [5], using complex diffusion filtering [12], wavelet transformations [5, 13, 14] among others.

In this paper we assess the potential use of several denoising filters in the reduction of speckle noise in

dermatological OCT imaging. We include in the evaluation well known 2D filters previously used in speckle reduction, such as versions of Enhanced Sigma (ES) [15], Adaptive Wiener (AW) [16] and Adaptive Wavelet Thresholding (AWT) [17] filters but also recent denoising filters with high edge-preserving capabilities like Non Local Means (NLM) [18] and Block Matching 3-D (BM3D) algorithm [19]. Finally we evaluate the combination of previous 2D filters with B-Scan Fusion based on wavelets decomposition (WFS) [20] and wavelet denoising considering multiple B-scans (WFM) [14] to assess the improvement of this strategy with respect to filtering single frames. We evaluate filter performance through common speckle-reduction performance metrics [5, 13, 21, 22] including Signal to Noise Ratio (SNR), Contrast to Noise Ratio (CNR), Equivalent Number of Looks (ENL) which is a measure of the smoothness of homogeneous regions of interest, and Edge-Enhancing Index (EEI) to assess the ability to enhance edges.

## 2. METHODS

### 2.1. Denoising filters

In the evaluation we have tested seven different denoising filters. Five of them (ES, AW, AWT, NLM and BM3D) are methods that are applied to individual B-scans. In addition we have applied other two B-scan compounding methods (WFS and WFM) to groups of two frames.

The Sigma Filter, also known as Lee Filter [23], is based on the two-sigma probability of Gaussian distribution and incorporates the speckle multiplicative noise model. Besides its simplicity it provides a good balance between filtering accuracy and computational complexity. We use an implementation that improves the preservation of small edges decomposing the image in several components and applying to them the sigma filter (ES). Adaptive Wiener filter (AW) calculates the local mean, the variance and the noise power estimation and uses these local statistics adaptively to generate a pixelwise Wiener filter. The Adaptive Wavelet Thresholding (AWT) performs a discrete wavelet transform and estimates the noise standard deviation from the detail coefficients at the first level, defines an adaptive threshold based on the previous estimation and a penalization method provided by Birgé-Massart, applies a global soft threshold to the coefficients and finally perform the inverse discrete wavelet transform [17]. The NLM method [18] uses a weighted averaging scheme to perform image denoising. The approach is to build a pointwise estimate of the image where each pixel is obtained as a weighted average of pixels centered at regions that are similar to the region centered at the estimated pixel. The estimates are non-local as in principle the averages can be calculated over all pixels in the image. A variation of NLM was proposed with the BM3D algorithm [19], based on an enhanced sparse representation in transform domain. The enhancement of the sparsity was achieved by grouping similar 2D fragments of the image into 3D data arrays (3D groups) and applying collaborative filtering to these groups.

Finally as we work with 3D volumes (sets of multiple B-scans), we have also evaluated two methods based on compounding strategies. The Image Fusion (WFS) based on wavelet decomposition transforms the original images (adjacent B-scans in our study) combines the coefficients on the transformed space and then applies the inverse transform to obtain the final result [20]. Finally the Wavelet Multiframe (WFM) algorithm [14] uses wavelet decompositions of single frames for a local noise and structure estimation. Based on this analysis, the wavelet detail coefficients are weighted, averaged and reconstructed. In both cases we use two consecutive frames (or B-scans) to perform the calculations.

### 2.2. Enhancement metrics

As defined in [5, 13, 21, 22] Signal to Noise Ratio (SNR) or Peak Signal to Noise Ratio is defined as:

$$\text{SNR} = 10 \log[ \max(I)2 / \sigma^2 ] \quad (1)$$

where  $I$  is the pixel value of the target OCT image, and  $\sigma^2$  is its noise variance. Contrast to Noise Ratio is:

$$\text{CNR} = (1/R) \sum_{r=1}^R (\mu_r - \mu_b) / \sqrt{\sigma_r^2 + \sigma_b^2} \quad (2)$$

where  $\mu_b$ ,  $\sigma_b^2$  are the mean and variance in a background noise region.  $\mu_r$ ,  $\sigma_r^2$  are the mean and variance of all regions of interest (R), including the homogeneous and heterogeneous regions of interest. Equivalent Number of Looks (ENL) is a measure of the smoothness of a homogeneous region of interest:

$$\text{ENL} = (1/H) \sum_{h=1}^H (\mu_h^2 / \sigma_h^2) \quad (3)$$

where  $\mu_h$ ,  $\sigma_h^2$  are the mean and variance of all homogeneous regions of interest (H). Except for the SNR calculations, all the other parameters were computed from logarithmic OCT images.

Finally Edge-Enhancing Index is defined as:

$$\text{EEI} = \frac{\sum_{n=1}^N |R_{f1} - R_{f2}|}{\sum_{n=1}^N |R_1 - R_2|} \quad (4)$$

where  $R_1$  and  $R_2$  represent the original values of the pixels on either side of the edge, and  $R_{1f}$  and  $R_{2f}$  are the corresponding filtered values over region of interest with edges (N).

## 3. EXPERIMENTS AND RESULTS

A dataset with 256 B-scans (1000x580 pixels) for the quantitative evaluation was acquired by scanning a dermatological human in-vivo tissue with a custom-designed spectral domain OCT system operating in the 1300 nm wavelength region. The broadband superluminescent diode operated at a center wavelength of 1320 nm and had a full-width at half-maximum bandwidth of 100 nm. The system was capable of providing axial and transverse resolutions of 8  $\mu\text{m}$  and 20  $\mu\text{m}$  respectively. Typical scanning dimensions covered a volume of 7x3.5x1.5  $\text{mm}^3$

(1024x512x1024 voxels). We perform the global evaluation of all the denoising filters in four steps.

The pre-processing step consists in the alignment of the image stack, adjusting each A-line of each image to keep the edge between the skin and the air constant in all the images.

The next step is the digital filtering of each B-scan before the B-scan compounding operation. For each individual B-scan the five digital filters described were applied: the ES Filter with a window size of 5 pixels, the AW Filter with window size of 5 pixels and a noise estimation based in the mode, the AWT Filter with the wavelet family Coiflet 2, a level of decomposition of 3, and an estimation of the noise based on the detail coefficients of the first level. The NLM used a kernel ratio of 4, a window ratio of 4 and filter strength of 0.06. The BM3D filter used a sharpening parameter of 1.11. The detail description of the previous parameters is beyond the scope of this paper. A complete description of these methods can be found in [14-20].

In the third step we apply the two proposed compounding filters (WFS and WMF) with groups of two adjacent B-scans previously filtered. For WFS we use the wavelet family Coiflet 1, the maximum fusion method for the approximation coefficients, the minimum for the details component and a level of decomposition equal to 6. For WFM we use 5 as decomposition levels, the Haar basis family,  $p$  controlling the noise reduction of 1.1 and as weight mode a combination of significance and correlation weights.

Finally we calculate the enhancement metrics (SNR, CNR, ENL and EEI) and display the results. The original raw B-scans have SNR, CNR and ENL mean±standard deviation values of 22.27±0.55 dB, 1.12±0.07, 82.15±3.42 respectively. Tables 1 and 2 show the subsequent improvement of the enhancement metrics with respect to these values except EEI which always compares the filtered and the original values (see (4)).

The results show that all the denoising filters improve the image quality metrics (SNR, CNR, ENL and EEI). The best results are accomplished using the combination of digital filtering individual B-scans followed by the image compounding of two adjacent B-scans using the WFM algorithm (Tables 1 and 2). With this strategy the enhancement metrics increase in all the filters and reduce the speckle noise, improving the possible study of details in the image (Figures 1 and 2).

Filter Name	SNR(dB)	CNR	ENL	EEI
ES	12.18 ±0.73	1.89±0.11	534±38	1.8±0.13
BM3D	12.28±0.72	1.77±0.06	475±42	1.65±0.06
AWT	10.73±0.47	1.74±0.05	468±27	1.33±0.07
AW	10.3±0.27	1.73±0.09	471±34	1.74±0.14
NLM	10.69±0.44	1.69±0.05	446±34	1.66±0.05

**Table 1.** Mean ± Standard Deviation of the improvement in the Enhancement metrics using the set of 256 dermatological OCT B-scans.

Filter Name	SNR(dB)	CNR	ENL	EEI
BM3D/WFM	17.28±1.73	3.25+0.23	1404±175	2.38±0.17
ES/WFM	16.8±1.12	3.21+0.15	1288±116	2.27±0.15
NLM/WFM	16.32±1.18	30.03+0.13	1166±112	2.31±0.16
AWT/WFM	16.47±1.17	3.01+0.21	1149±95	1.97±0.14
AW/WFM	15.96±0.94	2.95+0.15	1087±104	2.2±0.14
ES/WFS	14.8±0.64	2.9+0.14	1068±107	1.62±0.11
BM3D/WFS	16.1±1.32	2.96+0.21	1117±139	1.74±0.13
NLM/WFS	14.57±0.81	2.78±0.15	994±109	1.73±0.13
AWT/WFS	15.62±0.82	2.97±0.14	1089±124	1.52±0.12
AW/WFS	13.71±0.53	2.67±0.12	933±99	1.63±0.12

**Table 2.** Mean ± Standard Deviation of the improvement of the Enhancement metrics of the set of 256 dermatological OCT B-scans global process combining 2D denoising filters and compounding algorithms.

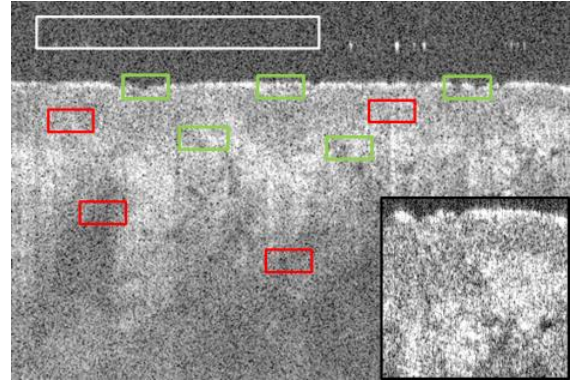


**Figure 1.** Dermatological OCT raw image before enhancement process B-Scan #1. Initial quality metrics SNR=21.89 dB, CNR=1.16, ENL=86.05 and EEI=4.34. ROIs used for the calculation of the quality ratios marked. White rectangle is used for noise estimation, red rectangles represent the homogeneous regions (H=4) and green rectangles the non-homogeneous regions, the three green rectangles at the top are used for the EEI (N=3). The sum of both are used to calculate the CNR (R=9).

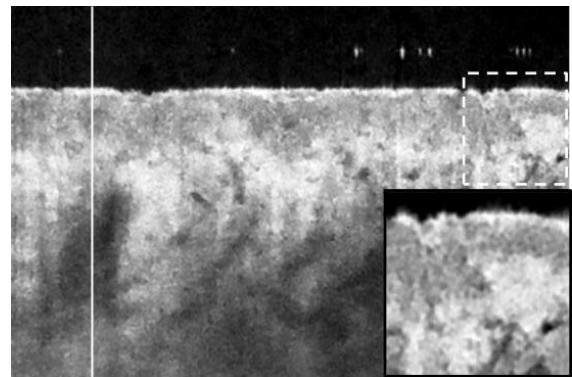


**Figure 2.** Dermatological OCT image (B-Scan #1) after applying the complete enhancement process with ES Filter followed by the WFM algorithm. Final quality metrics SNR=40.30 dB, CNR=41.57, ENL=1563.8 and EEI=12.99. Enhancement improvement values SNR=18.41 dB, CNR= 3.41, ENL=1447.7 and EEI=2.99. Vertical white line corresponds to A-Line #150.

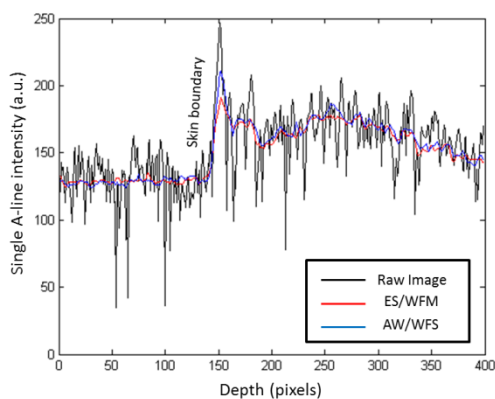


**Figure 3.** A-Line #150 profile of the Raw Image (black), the ES/WFM (red) and AW/WFS (blue) filtered B-Scan #1.

#### 4. CONCLUSIONS

The evaluation of several 2D denoising filters applied to dermatological OCT images shows an improvement in all the quality metrics used in the study (SNR, CNR, ENL and EEI). An additional step that compounds adjacent B-scans enables an extra enhancement and the consequent reduction of speckle noise without the need of an extra acquisition of the same frame. The 2D filters that show better performance in the study are the ES Filter and the BM3D in combination with the WFM. Further work must be done considering the evaluation of other compounding algorithms (like BM4D among others), the creation of a gold standard image to assess edge capabilities and the analysis of computing performance issues in the global process. The qualitative assessment by specialists is also needed to confirm that the proposed enhancement scheme helps in the diagnosis of skin diseases.

#### 5. ACKNOWLEDGMENTS

This work was partly supported by the European Union FP7 project BiopsyPen and the European Fund for Regional Development (FEDER).

#### 6. REFERENCES

[1] D. Huang, E. A. Swanson, C. P. Lin, J. S. Schuman, W. G. Stinson, W. Chang, M. R. Hee, T. Flotte, K. Gregory, and C. A. Puliafito, "Optical coherence tomography," *Science*, vol. 254, no. 5035, pp. 1178-1181, 1991.

[2] A. Alex, J. Weingast, B. Hofer, M. Eibl, M. Binder, H. Pehamberger, W. Drexler, and B. Povazay, "3D optical coherence tomography for clinical diagnosis of nonmelanoma skin cancers," *Imaging in Medicine*, vol. 3, no. 6, pp. 653-674, 2011.

[3] W. Drexler, and J. G. Fujimoto, *Optical coherence tomography: technology and applications*: Springer, 2008.

[4] A. Alex, J. Weingast, M. Weinigel, M. Kellner-Höfer, R. Nemecek, M. Binder, H. Pehamberger, K. König, and W. Drexler, "Three-dimensional multiphoton/optical coherence tomography for diagnostic applications in dermatology," *Journal of biophotonics*, vol. 6, no. 4, pp. 352-362, 2013.

[5] A. Ozcan, A. Bilenca, A. E. Desjardins, B. E. Bouma, and G. J. Tearney, "Speckle reduction in optical coherence tomography

images using digital filtering," *JOSA A*, vol. 24, no. 7, pp. 1901-1910, 2007.

[6] J. M. Schmitt, S. H. Xiang, and K. M. Yung, "Speckle in optical coherence tomography," *Journal of biomedical optics*, vol. 4, no. 1, pp. 95-105, 1999.

[7] M. Szkulmowski, I. Gorczynska, D. Szlag, M. Sylwestrzak, A. Kowalczyk, and M. Wojtkowski, "Efficient reduction of speckle noise in Optical Coherence Tomography," *Optics express*, vol. 20, no. 2, pp. 1337-1359, 2012.

[8] N. Iftimia, G. J. Tearney, and B. E. Bouma, "Speckle reduction in optical coherence tomography by "path length encoded" angular compounding," *Journal of biomedical optics*, vol. 8, no. 2, pp. 260-263, 2003.

[9] J. Yi, Q. Wei, H. F. Zhang, and V. Backman, "Structured interference optical coherence tomography," *Optics letters*, vol. 37, no. 15, pp. 3048-3050, 2012.

[10] M. Pircher, E. Götzinger, R. Leitgeb, A. Fercher, and C. Hitzenberger, "Measurement and imaging of water concentration in human cornea with differential absorption optical coherence tomography," *Optics Express*, vol. 11, no. 18, pp. 2190-2197, 2003.

[11] B. Sander, M. Larsen, L. Thrane, J. L. Hougaard, and T. M. Jørgensen, "Enhanced optical coherence tomography imaging by multiple scan averaging," *British Journal of Ophthalmology*, vol. 89, no. 2, pp. 207-212, 2005.

[12] D. Cabrera Fernández, H. M. Salinas, and C. A. Puliafito, "Automated detection of retinal layer structures on optical coherence tomography images," *Optics Express*, vol. 13, no. 25, pp. 10200-10216, 2005.

[13] D. C. Adler, T. H. Ko, and J. G. Fujimoto, "Speckle reduction in optical coherence tomography images by use of a spatially adaptive wavelet filter," *Optics letters*, vol. 29, no. 24, pp. 2878-2880, 2004.

[14] M. A. Mayer, A. Borsdorf, M. Wagner, J. Hornegger, C. Y. Mardin, and R. P. Tornow, "Wavelet denoising of multiframe optical coherence tomography data," *Biomedical optics express*, vol. 3, no. 3, pp. 572-589, 2012.

[15] R. C. Bilcu, and M. Vehvilainen, "A modified sigma filter for noise reduction in images."

[16] J. S. Lim, "Two-dimensional signal and image processing," *Englewood Cliffs, NJ, Prentice Hall, 1990, 710 p.*, vol. 1, 1990.

[17] S. G. Chang, B. Yu, and M. Vetterli, "Adaptive wavelet thresholding for image denoising and compression," *Image Processing, IEEE Transactions on*, vol. 9, no. 9, pp. 1532-1546, 2000.

[18] A. Buades, B. Coll, and J.-M. Morel, "A review of image denoising algorithms, with a new one," *Multiscale Modeling & Simulation*, vol. 4, no. 2, pp. 490-530, 2005.

[19] K. Dabov, A. Foi, V. Katkovnik, and K. Egiazarian, "Image denoising by sparse 3-D transform-domain collaborative filtering," *Image Processing, IEEE Transactions on*, vol. 16, no. 8, pp. 2080-2095, 2007.

[20] G. Pajares, and J. Manuel de la Cruz, "A wavelet-based image fusion tutorial," *Pattern recognition*, vol. 37, no. 9, pp. 1855-1872, 2004.

[21] D. L. Marks, T. S. Ralston, and S. A. Boppart, "Speckle reduction by I-divergence regularization in optical coherence tomography," *JOSA A*, vol. 22, no. 11, pp. 2366-2371, 2005.

[22] F. Qiu, J. Berglund, J. R. Jensen, P. Thakkar, and D. Ren, "Speckle noise reduction in SAR imagery using a local adaptive median filter," *GIScience & Remote Sensing*, vol. 41, no. 3, pp. 244-266, 2004.

[23] J.-S. Lee, "Digital image smoothing and the sigma filter," *Computer Vision, Graphics, and Image Processing*, vol. 24, no. 2, pp. 255-269, 1983.